Check for updates

Journal of Polymer Science

WILEY

JOURNAL OF POLYMER SCIENCE

RESEARCH ARTICLE OPEN ACCESS

Actuation and Charging Mechanisms of Thin PEDOT:PSS Films Probed by Electrochemical AFM and Impedance Spectroscopy

Tamino Rößler[1] | Matthias B. Engelhardt[1] | Nicolas Helfricht[1,2] | Georg Papastavrou[1,2,3]

[1]Department of Physical Chemistry II, University of Bayreuth, Bayreuth, Germany | [2]Bavarian Polymer Institute, University of Bayreuth, Bayreuth, Germany | [3]Bayreuth Center for Colloids and Interfaces, University of Bayreuth, Bayreuth, Germany

Correspondence: Georg Papastavrou (georg.papastavrou@uni-bayreuth.de)

Received: 15 January 2025 | **Revised:** 10 February 2025 | **Accepted:** 10 February 2025

Funding: This work was supported by the Studienstiftung des Deutschen Volkes, and the Elitenetzwerk Bayern.

Keywords: atomic force microscopy | electroactive polymers | soft matter actuators

ABSTRACT

PEDOT:PSS is a widely applied material in the field of organic electronics. Due to its mixed ionic-electronic conductivity, it is popular for soft actuators based on stimulated ion exchange. However, for confined spaces like thin films, interfaces play an important role in the actuation. Hence, we studied the actuation behavior of thin films of PEDOT:PSS with film thicknesses ranging from 100 nm up to 3 μm by atomic force microscopy. We observed a decrease in the relative expansion for thicker films. Moreover, the volume charge density also decreased. Electrochemical impedance spectroscopy granted more insight into film charging. We observed significant differences between oxidized and reduced films. We described ion diffusion by a pseudo-capacitance, which also decreased for thicker films. Hence, we conclude a limitation in thin PEDOT:PSS films affects the charging and the actuation.

1 | Introduction

Poly(3,4-ethylenedioxythiophene) (PEDOT), in combination with poly(4-styrenesulfonate) (PSS), is a widely used material for interfacing inorganic or organic electroactive materials [1–3]. The blend of PEDOT and PSS belongs to the class of mixed ionic-electronic conductors and exhibits a significant intrinsic electrical conductivity [4–6]. Moreover, PEDOT:PSS is increasingly used for signal transduction in the biomedical field [7, 8]. Due to its wide use, films from PEDOT:PSS have been thoroughly characterized in terms of conductivity, structure, and response to external potentials [4, 9–11]. Constructs from PEDOT:PSS have another interesting property, namely that they can act as actuators [12]. Generally, actuators are defined as components that allow for mechanical displacement or movement. The underlying mechanism for actuation is based on the oxidation and reduction of PEDOT, respectively. The reduction of PEDOT leads to a negative charge excess of the PSS anions, which results in an uptake of small hydrated cations from the solution, leading to a volume increase [13, 14]. This process is reversible upon oxidation of PEDOT.

So far, actuation processes of PEDOT:PSS have been primarily studied for thick micro- to millimeter-thick films [12, 15]. By contrast, the films that are commonly used for electrical interfacing electrical structures are much thinner, normally with a thickness in the nanometer range [16, 17]. Such electroactive polymer films can be structured laterally on the μm- and nm-scale and can be deposited by various techniques such as ink-jet printing and electropolymerization [14, 18, 19]. Hence, there has been considerable interest in utilizing them in the field of nano- and soft-robotics [15, 20]. Another field of application of such electroactive polymers is for the reversible actuation of micro- and nanopores [21, 22]. In light of these

This is an open access article under the terms of the Creative Commons Attribution License, which permits use, distribution and reproduction in any medium, provided the original work is properly cited.

© 2025 The Author(s). *Journal of Polymer Science* published by Wiley Periodicals LLC.

aforementioned applications, it is important to better understand the actuation mechanisms and physicochemical limits, such as the electromechanical coupling for thin films, which have a thickness below 1 μm. A central question is how far the behavior of thin electroactive polymer films is different from that of thicker films.

In order to study the electromechanical coupling of thin PEDOT:PSS films, atomic force microscopy (AFM) is a well-suited technique [2, 14]. AFM allows for time-resolved probing of the mechanical response on the nm level [13, 23–27]. As the actuation of electroactive polymers is based on the stimulated ion exchange with the bulk electrolyte solution, ion diffusion is a limiting parameter for fast response [28–31]. This ion diffusion in PEDOT:PSS can be probed by electrochemical impedance spectroscopy (EIS), which provides complementary information to spectroscopic ellipsometry that has been applied as well to thin PEDOT:PSS films [14, 19, 32, 33].

Here, we concentrated on the actuation behavior of thin PEDOT:PSS films prepared by electropolymerization on electrodes [34, 35]. The actuation has been probed in situ by AFM. The setup comprised an electrochemical 3-electrode setup incorporated into the liquid cell of the AFM [36]. By measuring the actuation response of PEDOT:PSS films, the electromechanical behavior of the thin films has been determined. These measurements have been complemented by EIS in the reduced and oxidized states. In this study, we address the question of how the charging and the actuation of thin PEDOT:PSS films scale with the film thickness.

2 | Results and Discussion

2.1 | Electropolymerization of PEDOT:PSS Films

Thin PEDOT:PSS films were prepared by electropolymerization under potentiodynamic conditions [37]. In order to obtain PEDOT:PSS films of different thickness h, the number of cycles n was varied between 3 and 50. Thicker films with $n > 50$ were also prepared. However, these films delaminated from the gold substrate even in an aqueous environment. The instability of thick PEDOT:PSS films is also reported in the literature [38]. Hence, we only prepared films with $n \leq 50$. Figure 1 shows the resulting evolution of the film thickness in the hydrated and in the dried state as a function of the number of cycles.

The thickness increases in both cases linearly with the number of cycles (cf. Figure 1a,b). The thickness of the thinnest film ($n = 3$) in the dried state was 50 nm. Each additional layer was on the order of 30 ± 1 nm. The thickness has been determined by measuring the depth of a scratch by AFM on freshly prepared films (cf. Figure 1c,d). The wet film thickness h_{wet} (cf. Figure 1b) corresponded directly to the dry thickness h_{dry} with a swelling factor $\chi = 2.3 \pm 0.1$ for an aqueous solution of 100 mM KCl. Thus, the thickness of the swollen films was in the range of 100 nm–3.5 μm. The linear relationship between the film thickness in the hydrated and dried states has also been observed for other hydrogel films, albeit with much higher swelling factors [39]. Hence, the small swelling factor indicates a relatively compact film structure, which is in line with studies on PEDOT:PSS electropolymerized under similar conditions [13].

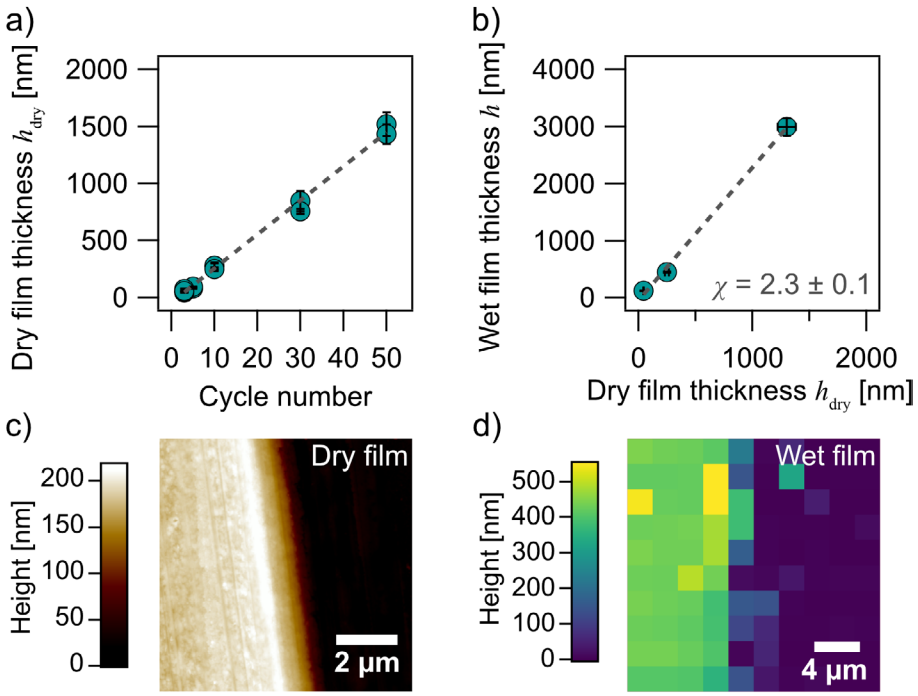

FIGURE 1 | Thickness of electropolymerized PEDOT:PSS films. (a) Film thickness h_{dry} in the dried state as a function of the number of cycles in the electropolymerization procedure. (b) Film thickness h in the hydrated, that is, wet state, as a function of the thickness in the dried state. The regression line gives the swelling factor χ. The measurements in the wet state have been performed in 100 mM KCl. (c) Topography of PEDOT:PSS with a scratch (right side) in the dried state as acquired by Tapping Mode under ambient conditions for a film prepared by $n = 10$ electropolymerization cycles. (d) Surface topography for a film prepared by $n = 10$ cycles in 100 mM KCl. The image has been acquired in force volume mode for a film with a scratch.

26424169, 2025, 21, Downloaded from https://onlinelibrary.wiley.com/doi/10.1002/pol.20250064 by Universitaet Bayreuth, Wiley Online Library on [10/03/2026]. See the Terms and Conditions (https://onlinelibrary.wiley.com/terms-and-conditions) on Wiley Online Library for rules of use; OA articles are governed by the applicable Creative Commons License

In order to corroborate the swelling behavior of the electrogelated films, the same film has been examined by AFM, one time in situ and one time in the dried state. Figure 1c,d shows the corresponding AFM height images in the dried state (cf. Figure 1c) and in the swollen state (cf. Figure 1d), respectively. It should be pointed out that in Figure 1 only an average film thickness has been reported. Furthermore, the film topography of electropolymerized PEDOT:PSS films was investigated by Tapping Mode AFM in air. Four exemplary AFM topography images in Figure 2 demonstrate that with an increasing number of cycles, the surface roughness of PEDOT:PSS films increased significantly.

This effect has been observed likewise for potentiostatically electropolymerized PEDOT:PSS films [40]. In the Supporting Information, the roughness as a function of cycles has been compiled for the films studied here. The surface morphology results from the PEDOT:PSS microstructure as short PEDOT chains align themselves alongside the longer PSS chains. The resulting polymer blend consists primarily of 30–50 nm particles bearing PEDOT-rich cores and PSS-rich shells [41]. This structure accounts for the electronic conductivity through the PEDOT domains and ion conductivity through the PSS domains [29].

2.2 | Electrochemical Actuation of PEDOT:PSS Films

Figure 3 schematically depicts the electrochemical actuation of a PEDOT:PSS film in an electrolyte environment. When PEDOT is oxidized, the positive charges in its backbone are compensated by the negative charges of PSS. The whole polymer is in a compact state. However, when the PEDOT gets reduced, the negative charge excess has to be compensated by migrating counterions from the surrounding electrolyte solution. This ion flux also draws water molecules into the polymer network. The resulting overall volume expansion of the film is based on the reversible oxidation/reduction process [13]. Consequently, the actuation process is also reversible, enabling the application of PEDOT:PSS films as actuators [42]. The described process of electrochemical actuation is common for mixed ionic-electronic conductors, not only PEDOT:PSS. However, large immobile macro-ions, like PSS, are important to mediate reversible cation-driven actuation [25, 43, 44]. In order to determine the electrochemically induced actuation of PEDOT:PSS films by AFM, we integrated an electrochemical cell into the AFM setup. A schematic representation is given in Figure 4a. The probe is pressed on the film and follows the actuation of the film due to the externally applied potential (cf. Figure 4c).

In contrast to other studies, we utilized the so-called colloidal probe technique, where the sharp AFM tip is replaced by a spherical colloidal particle [23–25, 45, 46]. Figure 4b shows a scanning electron microscopy (SEM) image of such a colloidal probe (CP). CPs allow for defined interaction geometries

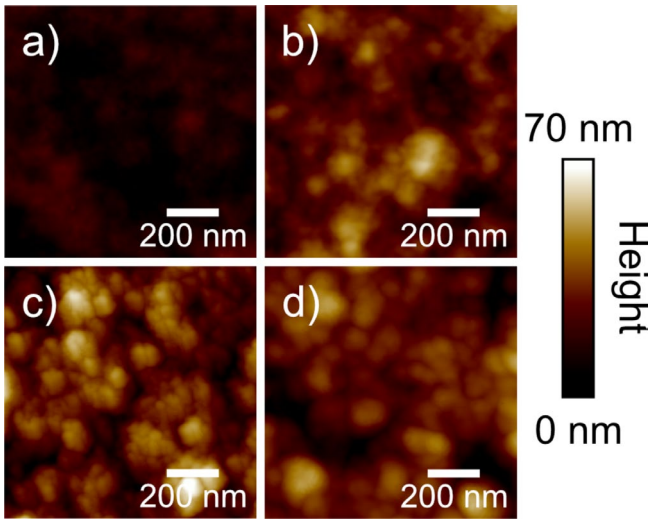

FIGURE 2 | Surface topography of PEDOT:PSS films acquired by Tapping Mode AFM in air for a scan size of $1 \times 1\,\mu m^2$. The different images illustrate how the film roughness increases with the number n of electropolymerization cycles. (a) $n = 5$; (b) $n = 10$; (c) $n = 30$; and (d) $n = 50$.

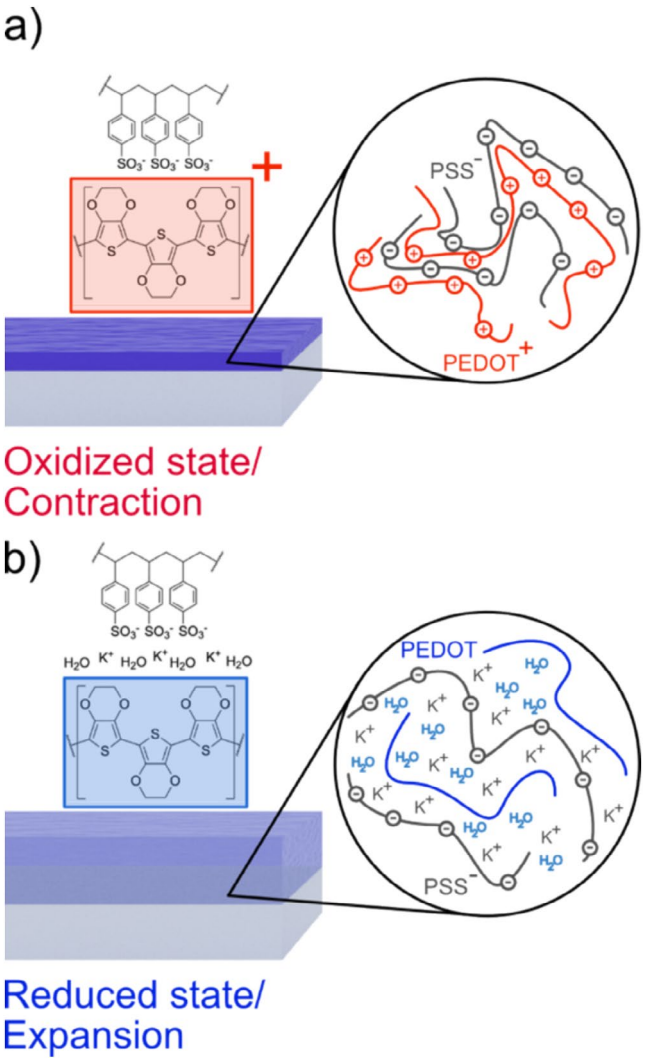

FIGURE 3 | Schematic representation of the overall state and the internal structure of a PEDOT:PSS film upon oxidation and reduction, respectively. (a) In the oxidized state, the positive charges of the PEDOT backbone are compensated by the PSS. (b) In the reduced state, the excess of negative charges from PSS can only be compensated by an uptake from solvated cations from the electrolyte solution. This process results in a volume increase and thus an actuation of a thin PEDOT:PSS film [13].

26424169, 2025, 21, Downloaded from https://onlinelibrary.wiley.com/doi/10.1002/pol.20250064 by Universitaet Bayreuth, Wiley Online Library on [10/03/2026]. See the Terms and Conditions (https://onlinelibrary.wiley.com/terms-and-conditions) on Wiley Online Library for rules of use; OA articles are governed by the applicable Creative Commons License

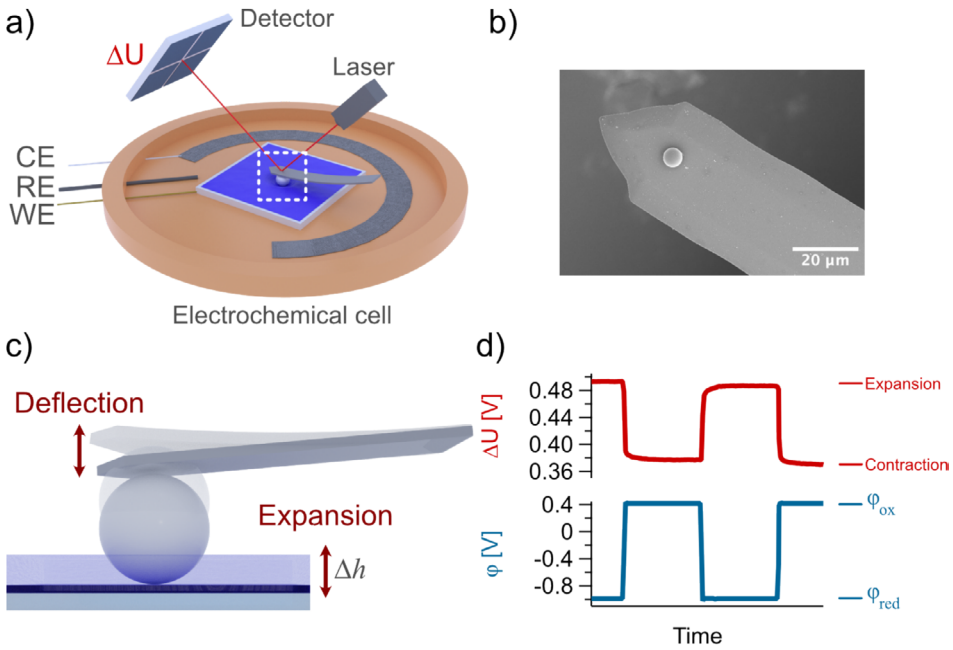

FIGURE 4 | (a) Schematic representation of the experimental setup for the combination of electrochemistry and force measurements by AFM. The potential applied to the PEDOT:PSS film was controlled by an external potentiostat and a 3-electrode electrochemical cell integrated into the AFM liquid cell. (b) SEM image of the colloidal probe used for the actuation experiments. (c) During the combined experiments, the relative height change Δh has been acquired by means of the deflection of the AFM cantilever. (d) The variation in the photodiode signal ΔU and the externally applied potential φ was acquired simultaneously.

between probe and sample. Moreover, due to their large contact area compared to sharp tips, they reduce the effect of surface roughness on the following measurements. Here, the CPs have been prepared by sintering silica particles to tipless Si-cantilevers [47].

In order to induce actuation of the PEDOT:PSS films, chronoamperometry has been used [23]. PEDOT:PSS was oxidized and reduced by applying alternating potential pulses φ_{ox} and φ_{red}, respectively. The potential φ remained constant for a certain time interval (cf. Figure 4d). Simultaneously to the electrochemical pulses, the cantilever deflection has been acquired by measuring the photodiode signal ΔU. The cantilever deflection, as determined by the light-lever method, can be readily converted to a travel of the probe in nanometers, based on the so-called inverse optical lever sensitivity (InvOLS) [48]. The InvOLS has been determined beforehand on a hard substrate. Figure 4d summarizes typical results for these chronoamperometric experiments in an AFM, showing the simultaneously acquired potential φ and the deflection signal ΔU from the cantilever due to the actuation of the PEDOT:PSS film (cf. Figure 4c). Separate chronoamperometry experiments were conducted in another electrochemical cell with defined electrode dimensions. This allowed for a quantitative analysis of the charge densities.

2.3 | Influence of the Applied Potentials

First, we studied how the externally applied potential φ_{red} influenced the film actuation. For these experiments, the oxidation potential was set to the constant value $\varphi_{ox} = +343$ mV (vs. Ag/AgCl), and the reduction potential φ_{red} has been varied between −456 mand −1056 mV (vs. Ag/AgCl). The film used for these experiments had a thickness of $h = 3.5\,\mu$m in the wet state as determined by AFM imaging of a scratch (cf. Figure 1d for an example). Here, we report the expansion Δh and the total charge density σ per surface area by varying φ_{red}. The latter has been determined in separate experiments by integrating the current over time and normalizing the resulting charge to the electrode area. For these experiments, the colloidal probe has been pressed against the PEDOT:PSS film with a constant fixed loading force of 1.7 µN. Then, the film was oxidized and reduced alternatingly. The mechanical response of the cantilever is measured simultaneously via the cantilever deflection. For that purpose, the feedback loop was turned off. We also conducted measurements with an enabled feedback loop. However, we observed no significant difference in the determined film expansions.

Figure 5 summarizes how film expansion and charge density varied with the applied reduction potential: Both Δh and σ increased monotonously with the magnitude of the reduction potential φ_{red}. This behavior indicated that increasing the magnitude of the reduction potential allowed for reducing a larger fraction of PEDOT in the film. Hence, more counter ions had to migrate for charge neutralization into the polymer film. Increasing the volume thus led to a larger expansion Δh of the film perpendicular to the substrate. Spectro-electrochemistry revealed that PEDOT can carry polarons or bipolarons, corresponding to one or two positive charges [10, 11]. At low reduction potentials (−400 mV vs. Ag/AgCl) a significant amount of polarons but no bipolarons are observed [11]. For higher reduction potentials (−600 mV vs. Ag/AgCl), the number of neutral states increases, but polarons can still be found [10, 11]. Hence, most likely even for high reduction potentials (–1 V vs. Ag/AgCl), PEDOT could be significantly charged, and the observed increasing expansion of the films (cf. Figure 5) is in line with

26424169, 2025, 21, Downloaded from https://onlinelibrary.wiley.com/doi/10.1002/pol.20250064 by Universitaet Bayreuth, Wiley Online Library on [10/03/2026]. See the Terms and Conditions (https://onlinelibrary.wiley.com/terms-and-conditions) on Wiley Online Library for rules of use; OA articles are governed by the applicable Creative Commons License

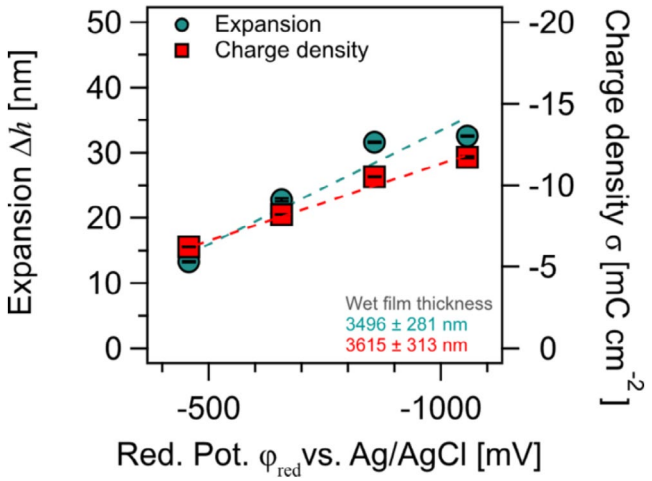

FIGURE 5 | Film expansion Δh and charge density per area σ as obtained from AFM/electrochemistry experiments and chronoamperometry, respectively, for different reduction potentials φ_{red}. The film thickness was, in both cases, on the order of 3.5–3.6 μm. All experiments were carried out in 100 mM KCl. The solid lines are guides to the eye only.

the increasing depletion of positive charges when the reduction potentials became more negative [10, 11]. Compared to a 3.5 μm thick PEDOT:PSS film, a thickness change of 30 nm is already a significant increase in film thickness. The oxidation potential φ_{ox} has not been varied to prevent film degradation. For oxidations at +800 mV (vs. Ag/AgCl), the films delaminated from the gold substrate.

2.4 | Influence of the Film Thickness

In another set of experiments, the thickness h of the PEDOT:PSS film has been varied while the oxidation and reduction potentials remained constant at $\varphi_{ox} = +343$ mV and $\varphi_{red} = -1057$ mV (vs. Ag/AgCl), respectively. The thickness h can be defined by the number of cycles carried out during potentiodynamic electropolymerization of PEDOT:PSS (cf. Figure 1a). Figure 6a summarizes the film expansion Δh and the derived charge density per area σ for film thicknesses from $h = 80$ nm ($n = 3$ cycles) to $h = 3.5$ μm ($n = 50$ cycles). Figure 6b shows the same data but normalized Δh to the respective film thickness h in the hydrated state as determined by AFM. It should be noted that the charge density per surface area converts in this way to a volume charge density ρ of the total charges injected in the film.

Figure 6 demonstrates that while the total expansion Δh and charge densities σ increased with film thickness h on an absolute scale (cf. Figure 6a) this is not valid for the same set of parameters when considering $\Delta h/h$ and ρ, respectively. Both, that is, $\Delta h/h$ and ρ, decrease with film thickness h (cf. Figure 6b). As the film thickness increases, more PEDOT is oxidized and reduced. However, the increase in Δh does not scale with the film thickness. Thus, the electrochemical process and the resulting expansion became increasingly ineffective: For a 3.5 μm-thick film, the total expansion was only about 3 times as large as for an 80 nm-thick film. A similar behavior has been reported for films prepared from polypyrrole:PSS [24].

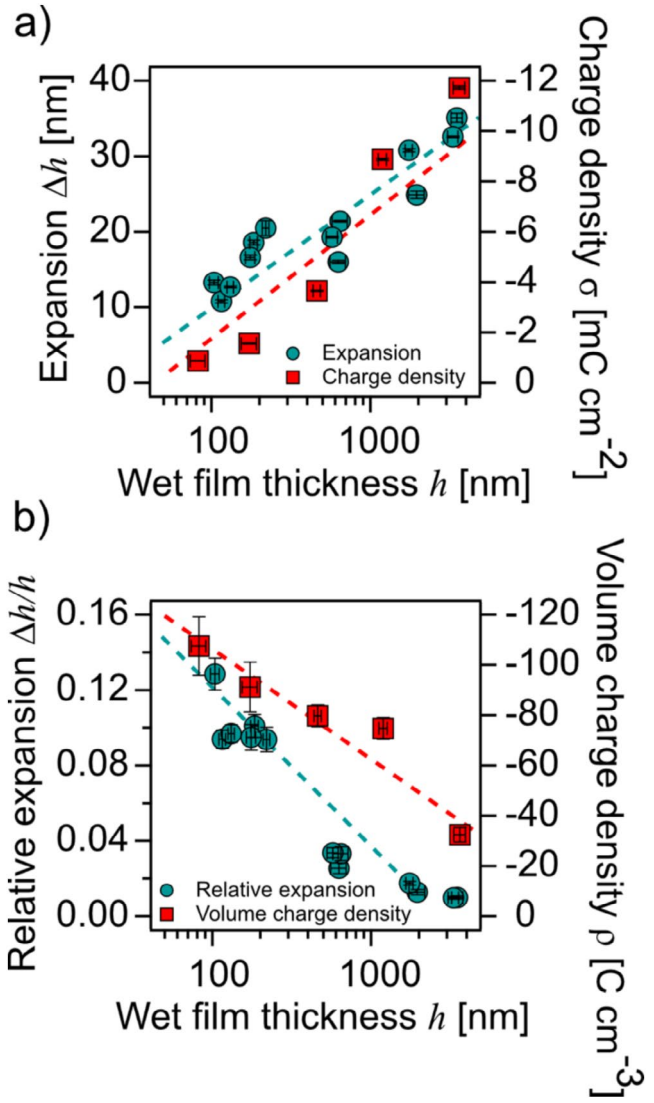

FIGURE 6 | (a) Film expansion Δh and charge density per area σ as obtained from AFM/electrochemistry experiments and chronoamperometry, respectively, for different film thicknesses h. Film actuation was carried out by square-wave voltammetry with $\varphi_{red} = -1057$ mV and $\varphi_{ox} = +343$ mV (vs. Ag/AgCl). All experiments were carried out in 100 mM KCl. (b) The same data as above but normalized to the film thickness h, resulting in a relative actuation and a volume charge density ρ. The solid lines are guides to the eye only.

The migration of ions into the film, which is responsible for the volume increase, is strongly related to diffusive transport [14]. For the latter, a diffusional time constant $\tau = h^2/4D$ can be attributed, which corresponds to the mass diffusion transport [24, 30]. This ion movement is initiated by oxidation and reduction at an electrode, which is strongly associated with an externally applied electrical field. The associated process is described in the framework of a so-called drift-diffusion model in moving-front experiments [30, 31, 49, 50]. A study on PEDOT:PSS films via the electrochemical quartz crystal microbalance (E-QCM) shows a cation gradient from the underlying electrode towards the electrolyte solution [51]. For sodium ions in PEDOT:PSS, the diffusion coefficient is about $7 \times 10^{-11} m^2 s^{-1}$ [52]. Hence, in a similar system with a film thickness of 10 μm, the response time would be smaller than

26424169, 2025, 21, Downloaded from https://onlinelibrary.wiley.com/doi/10.1002/pol.20250064 by Universitaet Bayreuth, Wiley Online Library on [10/03/2026]. See the Terms and Conditions (https://onlinelibrary.wiley.com/terms-and-conditions) on Wiley Online Library for rules of use; OA articles are governed by the applicable Creative Commons License

1 s. However, the applied pulses are in the order of 5 s. Thus, there should be enough time for sufficient ion diffusion into the film. Hence, these models seem not directly applicable to the description of thin film actuation. In electrolytes, the formation of an electrical double layer on bare electrodes is an ubiquitous process [36]. However, the diffuse layer influences the applied electric field on the length scale of the Debye length, which is in the order of a few nanometers [31, 53–55]. Hence, for larger film thicknesses, for example, organic field effect transistors, the charge accumulation occurs on larger time scales. By contrast, for thin films, charge accumulation dominates [31]. Charge accumulation at electrode interfaces has been reported primarily for "dry" semiconductors like poly(3-hexylthiophene) as the formation of space charges at the electrode interface decreases the charge carrier density with increasing film thickness [56]. In order to corroborate that charge accumulation is indeed responsible for the low relative actuation of thick films, we performed EIS. This technique allows for a deeper insight into the electronic processes during reduction and oxidation, respectively.

2.5 | EIS of Oxidized PEDOT:PSS Films

First, we studied the films in the oxidized state by EIS. EIS has been carried out at a DC offset of $\varphi_{ox} = +343$ mV versus Ag/AgCl and an AC amplitude of 10 mV. The DC offset corresponds to the oxidation potential used during the actuation experiments. The background electrolyte was 100 mM KCl. Similar parameters for EIS measurements have also been used for other electroactive polymer films in the oxidized state, as reported in the literature [57]. Figure 7a,b show the Bode plots compiled for the EIS measurements of oxidized PEDOT:PSS films of different thicknesses.

In the Bode plot of Figure 7b, a pronounced phase shift of nearly −90° has been observed. As the PEDOT:PSS film is compact in its oxidized state, we assume that the ion diffusion in the polymer films was significantly reduced [2, 51]. Therefore, diffusion has been neglected for the oxidized state as a first-order approximation, and we considered only the contributions due to the formation of internal electric double layers within the film. However, in contrast to purely capacitive behavior for flat metal electrodes, the nonuniformity of the internal film structure required more complex modeling, which is normally achieved by a constant phase element (CPE) [58, 59]. For oxidized PEDOT:PSS, the electric double layers are formed between PSS-rich domains and PEDOT-rich domains in the film [54]. The microstructure of the PEDOT:PSS film shows an intertwined arrangement of PEDOT-rich and PSS-rich domains (cf. Figure 3) [41, 54]. The CPE labeled CPE_{edl} allowed accounting for this structure of the diffuse layer within the film [60]. The parameter α indicates to which extent the CPE shows a primarily capacitive behavior within the equivalent circuit. The phase deviation θ from a "pure" capacitance, which shows a phase shift of 90°, is given for a CPE by:

$$\theta = 90^{\circ} \bullet (1 - \alpha) \tag{1}$$

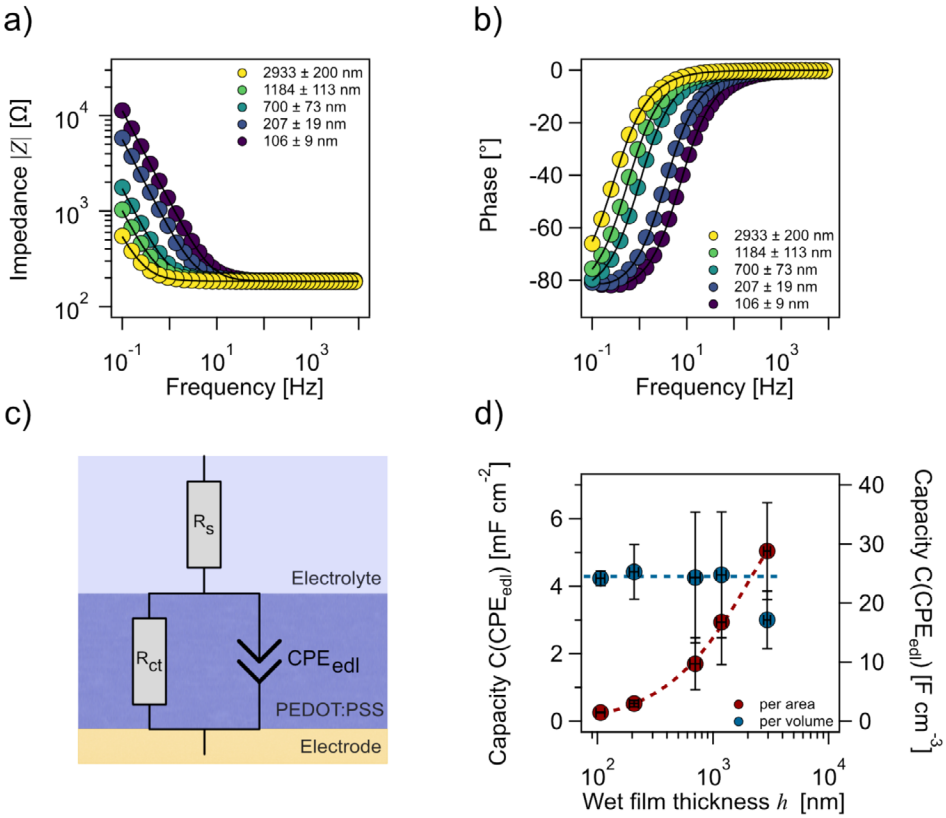

FIGURE 7 | Electrochemical impedance spectroscopy (EIS) of PEDOT:PSS films in the oxidized state of different thicknesses. (a) Bode plot for the magnitude of impedance Z and (b) phase shift. The EIS data were acquired at $\varphi_{ox} = +343$ mV (vs. Ag/AgCl) and an amplitude of 10 mV. (c) Equivalent circuit for the film in the oxidized state. (d) Capacitance as derived from the values for CPE_{edl}, normalized to area and volume.

26424169, 2025, 21, Downloaded from https://onlinelibrary.wiley.com/doi/10.1002/pol.20250064 by Universitaet Bayreuth, Wiley Online Library on [10/03/2026]. See the Terms and Conditions (https://onlinelibrary.wiley.com/terms-and-conditions) on Wiley Online Library for rules of use; OA articles are governed by the applicable Creative Commons License

For $\alpha = 1$, the CPE acts as a capacitor, while for $\alpha = 0$, the CPE acts as a resistor [58]. The electron transfer resistance R_{ct} is placed in parallel to the capacitive contributions of CPE, as commonly encountered for a simplified Randles circuit in combination with R_s for the solution and cable resistance [59]. The EIS spectra have been quantitatively evaluated by means of an equivalent circuit shown in Figure 7c and the resulting fits are shown as solid lines in Figure 7a,b.

The results from fitting the EIS spectra to the equivalent circuit are shown in Figure 7c. Further fitting results are summarized in the SI for all films studied. The α of CPE_{edl} remained close to 1 for all film thicknesses studied here (cf. Figure S5). Hence, a dominantly capacitive behavior within the film can be assumed. The thereby determined capacity $C(CPE_{edl})/A$ increased with film thickness as summarized in Figure 7d when the results are only normalized to the surface area A of the electrode. However, if the capacity is normalized to the total volume of the film as given by the area A and the film thickness h, the resulting volume capacity, $C(CPE_{edl})/V$, remained constant independently of the film thickness. This finding supports the interpretation of CPE_{edl} as internal diffuse layer capacity for the PEDOT-rich regions in the film. It is known that the total capacity of PEDOT:PSS films has to be viewed as containing some small three-dimensional capacitors [54]. Hence, an increasing thickness leads to higher capacities. However, the constant capacitance per volume corroborates the assumption of diffuse layers. Moreover, its capacity fell within the range of 10–100 F cm^{-3}, which is in line with values reported in the literature [54].

2.6 | EIS of Reduced PEDOT:PSS Films

The PEDOT:PSS films in the reduced state were studied by a DC offset of $\varphi_{red} = -1057$ mV versus Ag/AgCl and an AC amplitude of 10 mV, which also resembles previous studies reported in the literature of comparable systems [57]. The DC offset corresponds to the reduction potential used for the actuation experiments. The corresponding EIS spectra represented by the Bode plots are shown in Figure 8a,b.

It is evident that for the reductive state, the frequency-dependent behavior was more complex than for the films in the oxidized state. In Figure 8b, two phase shifts are visible in the Bode plot. The first shift at higher frequencies shows no dependence on the film thickness. However, the second shift at lower frequencies depends on the film thickness. The occurrence of the second shift in Figure 8b has been considered by the addition of a second CPE_{diff}, which relates to diffusion within the film with respect to faradaic currents [60]. The corresponding equivalent circuit, including two CPEs, is shown in Figure 8c. Analogous equivalent circuits have been utilized in the past for similar systems [60, 61].

The results for the fits to the equivalent circuit (cf. Figure 8c) are summarized in the SI. In contrast to the oxidized state, the

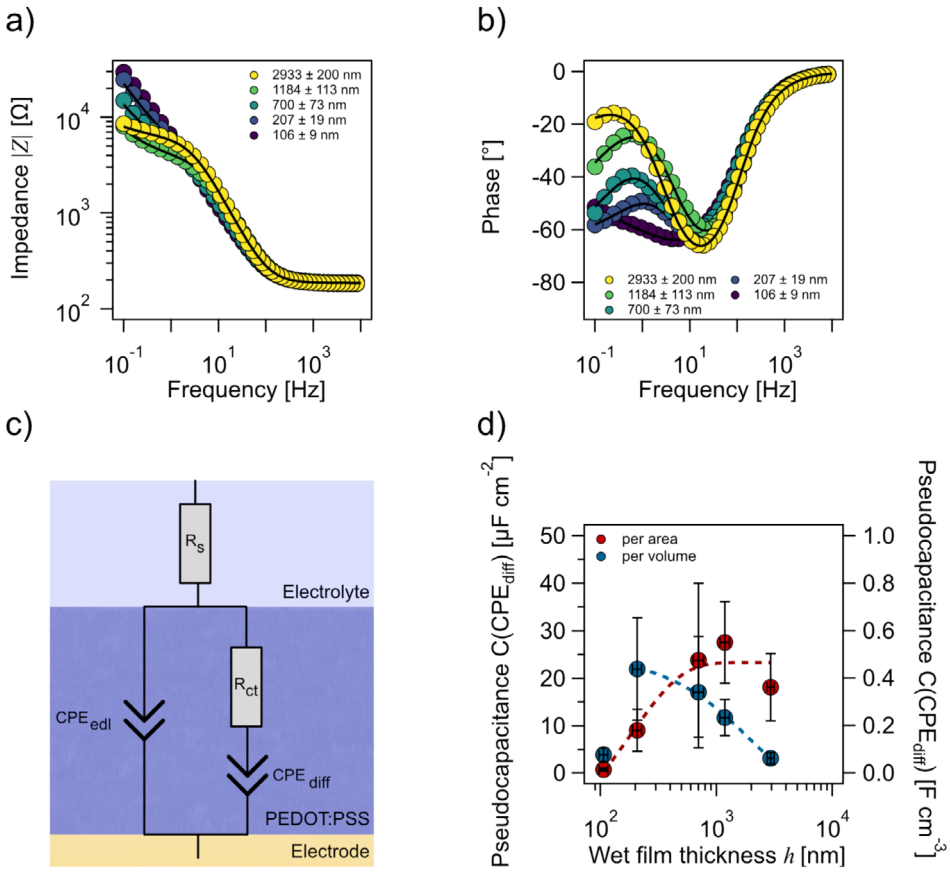

FIGURE 8 | Electrochemical impedance spectroscopy (EIS) of PEDOT:PSS films in the reduced state of different thicknesses. (a) Bode plot for the magnitude of impedance Z and (b) phase shift. The EIS data were acquired at $\varphi_{red} = -1057$ mV (vs. Ag/AgCl) and an amplitude of 10 mV. (c) Equivalent circuit for the film in the reduced state. (d) Pseudo-capacitance as derived from the values for CPE_{diff} normalized to area and volume.

26424169, 2025, 21, Downloaded from https://onlinelibrary.wiley.com/doi/10.1002/pol.20250064 by Universitaet Bayreuth, Wiley Online Library on [10/03/2026]. See the Terms and Conditions (https://onlinelibrary.wiley.com/terms-and-conditions) on Wiley Online Library for rules of use; OA articles are governed by the applicable Creative Commons License

values for CPE_{edl} remained approximately constant for all film thicknesses studied here (cf. Figure S5b). We assume that this difference from the oxidized state results from the counter-ions incorporated in the film. In the reduced state, cations from the electrolyte solution have migrated into the polymer film for charge compensation of PSS anions. The α for CPE_{edl} remained nearly equal to 1 for all films (cf. Figure S5c). Hence, as CPE_{edl} describes again a primarily capacitive charging and is independent of the film thickness (cf. Figure S5b), the contributions to diffuse layer capacity $C(CPE_{edl})$ must arise primarily from the Au electrode rather than the PEDOT:PSS film.

By contrast, the second CPE, namely CPE_{diff}, has been attributed to the behavior of mobile cations within the film, which is primarily diffusive in nature and contributes to the charge transfer. Our results show that for CPE_{diff}, the values of α were ranging from 0.5 to 0.7 (cf. Figure S5a). Hence, they fall in a completely different regime than for CPE_{edl}. The cases of semi-infinite diffusion ($\alpha = 0.5$) and a reflective boundary ($\alpha = 1$) represent the extreme boundary conditions [58]. Pure diffusive behavior of an electroactive species is described by a Warburg element, which would correspond to $\alpha = 0.5$ for a CPE [58]. Thin films can have significant charge accumulation at the polymer/electrode interface, while the solid electrode acts as a reflective boundary [31, 58]. Therefore, we assume most of the ions move within the film and are not accumulated at the electrode. The diffusion alongside the PSS-rich domains results in a hindrance, leading to $\alpha < 1$. By contrast, for $\alpha \simeq 1$, we would expect basically charge accumulation at the Au electrode, which acts as a reflective boundary.

2.7 | Film Structure and Actuation Behavior

The EIS data allow for better matching of the actuation behavior with the film structure. The expansion of the PEDOT:PSS film upon reduction is attributed to the incorporation of the cations in the film in order to compensate for the charges of the PSS-rich regions [51]. For thin films, the expansion has been followed in an indirect manner, either by spectroscopic ellipsometry or by QCM [32, 33, 51]. Additionally, direct approaches like AFM-based experiments can be used [23, 25].

The reduced relative expansion observed for the thicker films, as determined by direct force measurements by AFM, can be related to the charge distribution in the films (cf. Figure 6b). Chronoamperometry showed a reduced volume charge density in the reduced state with increasing film thickness. One possible explanation would be a decrease in mass density with increasing film thickness during electropolymerization. However, the linear increase of the film thickness in the collapsed state (cf. Figure 1a) and the constant capacitance normalized to the volume in the oxidized state makes such a film structure unlikely (cf. Figure 7c) and suggest a homogeneous density profile in terms of polymer mass. However, in the reduced state, we find that the pseudo-capacity with respect to α decreases with increasing film thickness. Such a dependence indicates that finite diffusion of cations in the PEDOT:PSS film changes with film thickness, leading to nonhomogeneous charge accumulation within the film. Here, the extent of the PSS-rich regions might play an important role. The cations move alongside ionic conductor domains (i.e., PSS-rich domains) which hinders movements in contrast to the bulk solution. Hence, the cation diffusion takes place on long-time scales. One reason for the difference to macroscopic films could be the significant influence of the gold electrode due to the low film thickness, which could have an influence on the ion uptake. The influence of the Au electrode became most evident for the lowest film thickness in Figure 8d.

Throughout this study, DC signals have been applied. By contrast, Bonafé et al. studied the actuation behavior of similar polymer films by combining AFM and EIS [14, 62]. They showed a higher cation concentration towards the polymer-electrolyte interface for thin films of polypyrrole dodecylbenzenesulfonate (PPy:DBS), which they assumed to be linked to morphological changes in the polymer. However, PEDOT:PSS shows no morphological changes and a homogeneous ion distribution [62]. The swelling of PEDOT:PSS is supposed to be linked purely to the uptake of hydrated cations [14]. One possible explanation would be that the DC potentials do not allow for an unhindered counterion exchange.

3 | Conclusions

Since PEDOT:PSS and other conjugated polymers are widely used materials, not only as actuators but also as interface layers in organic electronics, the charging and actuation of thin films of PEDOT:PSS are of general interest for a number of fields. This study was based on electropolymerized PEDOT:PSS films on Au electrodes.

In contrast to previous studies, we determined the thickness change in thin films directly by electrochemical AFM and not by indirect techniques, such as ellipsometry and QCM. Additionally, we varied the film thickness in a defined manner by electropolymerization. Thereby, the influence on ion migration in the film and effects such as surface roughness could be included. By utilizing chronoamperometric methods and direct force measurements by AFM, we could demonstrate that thin films also show actuation with respect to their thickness, but that this actuation was on the order of 1%–16% of the total film thickness and decreased with increasing film thickness. This decrease in relative actuation coincides with a reduced volume charge density that can be attributed to the reduced diffusion of counterions in the film in the reduced state.

We found that higher reduction potentials lead to larger expansions. However, we observed that the expansion normalized to the respective film thickness decreased with increasing film thickness. This observation could be rationalized based on the decrease of charge density per volume with increasing thickness as derived from chronoamperometry and a nonhomogeneous charge distribution as derived from EIS. However, combined studies of AFM and electrochemistry from the literature indicate a homogeneous ion distribution for PEDOT:PSS but not for PPy:DBS [14, 62]. By contrast, E-QCM indicates a cation accumulation towards the electrode for PEDOT:PSS [51]. This charge accumulation is the reason for a hindered ion uptake in thicker films. Hence, film structure and geometry might play an important role in charge distribution and thus the actuation

26424169, 2025, 21, Downloaded from https://onlinelibrary.wiley.com/doi/10.1002/pol.20250064 by Universitaet Bayreuth, Wiley Online Library on [10/03/2026]. See the Terms and Conditions (https://onlinelibrary.wiley.com/terms-and-conditions) on Wiley Online Library for rules of use; OA articles are governed by the applicable Creative Commons License

behavior. For the here-prepared films by electropolymerization, the relation between the uneven charge distribution and actuation for thin films presents a limit to the actuation behavior of nm-scaled soft actuator devices. This limit would have important consequences for some applications, such as nano-release from films or switchable nano-pores [22, 63].

4 | Experimental Section/Methods

4.1 | Materials

Aqueous solutions were prepared with Milli-Q water (resistivity: 18.2 MΩ cm; Merck KGaA, Darmstadt, Germany). 3,4-ethylenedioxythiophene (EDOT, 97%, Sigma Aldrich, St. Louis, MO, USA), poly(sodium-4-styrenesulfonate) (NaPSS, $M_w = 70{,}000\,g\,mol^{-1}$, Sigma Aldrich, St. Louis, MO, USA), and potassium chloride (≥99.5%, Sigma Aldrich, St. Louis, MO, USA) were used as received. Ethanol and acetone (p.a., VWR Chemicals, Radnor, PA, USA) were used as recieved.

4.2 | Sample Preparation

Gold substrates were prepared via vapor deposition (Tectra GmbH, Frankfurt a. M., Germany) on glass. Glass slides ($11 \times 11\,mm^2$, Glasagentur Glenewinkel, Duingen, Germany) were sonicated in an aqueous solution of 2% (v/v) Hellmanex III (Helma, Müllheim, Germany) for 15 min at 40°C and rinsed with Milli-Q water. The slides were coated with chromium (thickness: 2 nm adhesive layer) and gold (thickness: 100 nm, Agosi AG, Pforzheim, Germany). The glass slides were partially masked during the coating process. The gold substrates were contacted via colloidal silver paste (MicroToNano, ET Haarlem, Netherlands) to a Teflon-isolated silver wire (Advent Research Materials Ltd., Witney, UK). Mechanical stability of the contact was improved via encapsulation of the contact point with UV-curing glue (NOA63, Norland Products Inc., Jamesburg, NJ, USA). A three-electrode setup was integrated into an electrochemical cell [36]. The gold substrates were acting as the working electrode (WE). The counter electrodes (CE) were fabricated from a platinum mesh arranged circularly around the WE. A chlorinated silver wire (Ag/AgCl), prepared with an automated chlorider (ACL-01, npi electronic GmbH, Tamm, Germany), was used as a reference electrode. Its potential shift has been determined versus a commercial Ag/AgCl electrode (3 M NaCl, BASi, West Lafayette, IN, USA).

Thin films of PEDOT:PSS were prepared freshly prior to every measurement via electropolymerization after a modified procedure of Knittel et al. [37]. The gold electrodes were cleaned by treatment with a Snow-Jet (30A Gunjet, Spraying Systems Co., IL, USA). Then, the polymer films were prepared by potentiodynamic electropolymerization from an aqueous solution of 10 mM EDOT, 0.1 mM NaPSS (based on M_w), and 100 mM KCl. The potential was cycled from −0.6 to 1 V (vs. Ag/AgCl) at $100\,mV/s^{-1}$ for 3, 5, 10, 30, and 50 cycles, respectively. Directly after preparation, the films were rinsed with an aqueous solution of 100 mM KCl. They were used immediately for the corresponding experiments. The pH value was not adjusted and was between pH 5 and 6.

4.3 | Colloidal Probe Preparation

Tipless ACT-TL cantilevers (no backside coating, nominal resonance frequency $f_{nom} = 300\,kHz$, nominal spring constant $k_{nom} = 37\,N\,m^{-1}$, Applied NanoStructures Inc., Mountain View, CA, USA) were cleaned with Milli-Q water, ethanol, acetone, ethanol, and Milli-Q water. Afterwards, they were treated with air plasma (Zepto, Diener electronic GmbH & Co KG, Ebhausen, Germany) for 3 min. Cantilever calibration was carried out in air by the thermal noise method using a MFP-3D atomic force microscope equipped with an ARC2 controller (Oxford Instruments Asylum Research, Santa Barbara, USA) [64]. For the used cantilever, we determined spring constants between 20 and $30\,N\,m^{-1}$. For calibration, the inverse optical lever sensitivity (InvOLS) was determined on a glass substrate cleaned by treatment with a Snow-Jet (30A Gunjet, Spraying Systems Co., IL, USA) and air plasma for 3 min. At least 30 force-versus-distance curves (3 spots à 10 curves) were acquired with a 1 μm scan range, $1\,\mu m\,s^{-1}$ velocity, 0.5 Hz scan rate, 0.1 V engage setpoint, and 0.2 V trigger setpoint.

Colloidal probes were prepared by sintering, that is, without glue, according to [47]. Prior to attaching the colloidal particles, the tipless cantilevers were treated with air plasma for 3 min. Micromanipulation has been performed with a DC-3 K micromanipulator (Maerzhaeuser GmbH & Co KG, Wetzlar, Germany) and controlled under a fixed-stage optical microscope (Axio Examiner, Carl Zeiss AG, Oberkochen, Germany). For the temporary immobilization, glycerol (≥99%, Fisher Scientific Inc., Loughborough, UK) was mixed with Ludox-TM50 particles (Sigma Aldrich, St. Louis, MO, USA) in a 3:2 (wt/wt) mixture. A small droplet was placed on the free end of the cantilever using an etched tungsten wire. Next, a single silica particle ($Ø_{nom}$ 6.8 μm, Bangs Laboratories Inc., Fishers, IN, USA) was placed on the droplet using another etched tungsten wire. The colloidal probes were sintered at 1200°C for 2 h (L5/12/B180, Nabertherm GmbH, Lilienthal, Germany) and then let cool down overnight.

4.4 | Film Actuation Probed by AFM

All actuation experiments by AFM were carried out on a MFP-3D atomic force microscope equipped with an ARC2 controller (Oxford Instruments Asylum Research, Santa Barbara, USA). Samples were prepared freshly prior to the actuation experiments. The electrochemical cell with the mounted sample was rinsed with an aqueous solution of 100 mM KCl before the experiments. The experiments were carried out in fresh electrolyte solution (100 mM KCl, the pH-value was not adjusted). The colloidal probes were cleaned before mounting by immersion in a series of solvents (Milli-Q water, ethanol, acetone, ethanol, and Milli-Q water) as well as by treatment with air plasma for 3 min. Before and after the actuation experiments, the InvOLS was determined on the glass area next to the polymer film (i.e., the area intentionally not covered during Au-evaporation). At least 300 force-versus-distance curves (3 spots à 100 curves) were recorded with the following parameters: 0.5 μm scan range, 1 Hz scan rate, $1\,\mu m\,s^{-1}$ velocity, and 0.3 V trigger−/engage setpoint. The InvOLS was evaluated with a custom-written Igor Pro procedure (Igor Pro 8.04, Wavemetrics, Portland, OR, USA). For the actuation experiments, the colloidal probe indented the

26424169, 2025, 21, Downloaded from https://onlinelibrary.wiley.com/doi/10.1002/pol.20250064 by Universitaet Bayreuth, Wiley Online Library on [10/03/2026]. See the Terms and Conditions (https://onlinelibrary.wiley.com/terms-and-conditions) on Wiley Online Library for rules of use; OA articles are governed by the applicable Creative Commons License

PEDOT:PSS film with an engage setpoint of 0.4 V. The feedback loop has been disabled. Alternating oxidation and reduction of the film has been induced by square-wave voltammetry (PGU BI-1000, IPS Elektroniklabor GmbH & Co KG, Münster, Germany). Various potential combinations were applied. At least 120 pulses were recorded (40 pulses at 3 spots). The potential and current output of the potentiostat were fed directly via the AUX channel into the ARC2 controller and saved in the same file as other data from the force versus distance curves. The pulse sequences were evaluated with a custom-written Igor Pro procedure.

4.5 | Chronoamperometry

Chronoamperometry experiments were performed separately from the actuation experiments. Freshly prepared samples were mounted in an electrochemical cell (TSC Surface, RHD instruments GmbH & Co KG, Darmstadt, Germany). The PEDOT:PSS sample acted as the WE, a chlorinated silver wire acted as a reference electrode, and a piece of glassy carbon acted as the CE. All experiments were carried out in an aqueous solution of 100 mM KCl (the pH-value was not adjusted). A circular area of the sample with a 0.35 cm radius was exposed to the electrolyte solution. Square-wave voltammetry (PGU BI-1000, IPS Elektroniklabor GmbH & Co KG, Münster, Germany) was performed for alternating oxidation and reduction. 20 pulses were applied for each potential combination. The data was evaluated with a custom-written Igor Pro procedure.

4.6 | Electrochemical Impedance Spectroscopy

EIS was conducted with a dedicated electrochemical workstation (Zennium, Zahner Elektrik GmbH & Co KG, Kronach, Germany) with the same electrochemical cell as for chronoamperometry in a Faraday cage. Oxidation and reduction were obtained by DC offsets (+343 mV and −1057 mV vs. Ag/AgCl, respectively). An AC signal with an amplitude of 10 mV was applied. The frequency range was 10 mHz to 100 kHz. Data evaluation has been performed with the Zahner Analysis software (Version 3.2.1, Zahner-Elektrik GmbH & Co KG, Kronach, Germany).

4.7 | Film Characterization

The film thickness has been determined in situ and in the dried state by obtaining height scans of a scratch in the PEDOT:PSS film. In the dry state, the measurements were done in Tapping Mode in air by a Dimension Icon equipped with a Nanoscope V controller (Bruker, Billerica, MA, USA) and AC160-TS cantilevers (Olympus, Tokyo, Japan, $f_{nom} = 300$ kHz, $k_{nom} = 26$ N m^{-1}) were used. The AFM images were evaluated with the NanoScope Analysis software (Version 1.8, Bruker, Billerica, MA, USA). In-situ measurements were carried out in an aqueous solution of 100 mM KCl with a MFP-3D equipped with an ARC2 controller. The colloidal probes used for the actuation experiments were also applied for imaging, which was carried out by so-called force volume plots [65]. The image analysis was done with the Asylum Research software (Version 16.33.234, Oxford Instruments Asylum Research, Santa Barbara, USA).

Acknowledgments

The authors acknowledge the help of the Keylab for Electron Microscopy of the Bavarian Polymer Institute and thank Paul Markus (University of Bayreuth) for programming an evaluation procedure in IgorPro. Tamino Rößler is grateful for the financial support of the Studienstiftung des deutschen Volkes and the Marianne-Plehn program. Tamino Rößler and Matthias B. Engelhardt thank for the support of the Elite Network of Bavaria within the study program "Macromolecular Science" and the University of Bayreuth graduate school.

References

1. J. Karst, M. Floess, M. Ubl, et al., "Electrically Switchable Metallic Polymer Nanoantennas," *Science* 374 (2021): 612–616.

2. F. Amorini, I. Zironi, M. Marzocchi, et al., "Electrically Controlled "Sponge Effect" of PEDOT:PSS Governs Membrane Potential and Cellular Growth," *ACS Applied Materials and Interfaces* 9 (2017): 6679–6689.

3. E. Cheah, M. Bansal, L. Nguyen, et al., "Electrically Responsive Release of Proteins From Conducting Polymer Hydrogels," *Acta Biomaterialia* 158 (2023): 87–100.

4. X. Crispin, F. L. E. Jakobsson, A. Crispin, et al., "The Origin of the High Conductivity of Poly(3,4-ethylenedioxythiophene)−Poly(Styrenesulfonate) (PEDOT−PSS) Plastic Electrodes," *Chemistry of Materials* 18 (2006): 4354–4360.

5. J. Huang, P. F. Miller, J. C. De Mello, A. J. De Mello, and D. D. C. Bradley, "Influence of Thermal Treatment on the Conductivity and Morphology of PEDOT/PSS Films," *Synthetic Metals* 139 (2003): 569–572.

6. H. J. Lee, J. Lee, and S. M. Park, "Electrochemistry of Conductive Polymers. 45. Nanoscale Conductivity of PEDOT and PEDOT:PSS Composite Films Studied by Current-Sensing AFM," *Journal of Physical Chemistry. B* 114 (2010): 2660–2666.

7. K. Roshanbinfar, M. Schiffer, E. Carls, et al., "Electrically Conductive Collagen-PEDOT:PSS Hydrogel Prevents Post-Infarct Cardiac Arrhythmia and Supports hiPSC-Cardiomyocyte Function," *Advanced Materials* 36, no. 28 (2024): e2403642, https://doi.org/10.1002/adma.202403642.

8. K. Roshanbinfar, L. Vogt, B. Greber, et al., "Electroconductive Biohybrid Hydrogel for Enhanced Maturation and Beating Properties of Engineered Cardiac Tissues," *Advanced Functional Materials* 28, no. 42 (2018): 1803951, https://doi.org/10.1002/adfm.201803951.

9. E. Hosseini, V. Ozhukil Kollath, and K. Karan, "The Key Mechanism of Conductivity in PEDOT:PSS Thin Films Exposed by Anomalous Conduction Behaviour Upon Solvent-Doping and Sulfuric Acid Post-Treatment," *Journal of Materials Chemistry C* 8 (2020): 3982–3990.

10. B. D. Paulsen, R. Wu, C. J. Takacs, et al., "Time-Resolved Structural Kinetics of an Organic Mixed Ionic–Electronic Conductor," *Advanced Materials* 32 (2020): e2003404.

11. G. Rebetez, O. Bardagot, J. Affolter, J. Réhault, and N. Banerji, "What Drives the Kinetics and Doping Level in the Electrochemical Reactions of PEDOT:PSS?," *Advanced Functional Materials* 32, no. 5 (2022): 2105821, https://doi.org/10.1002/adfm.202105821.

12. Y. Li, R. Tanigawa, and H. Okuzaki, "Soft and Flexible PEDOT/PSS Films for Applications to Soft Actuators," *Smart Materials and Structures* 23 (2014): 074010.

13. S. Benaglia, S. Drakopoulou, F. Biscarini, and R. Garcia, "In Operandonanomechanical Mapping of PEDOT:PSS Thin Films in Electrolyte Solutions With Bimodal AFM," *Nanoscale* 14 (2022): 14146–14154.

14. F. Bonafè, F. Decataldo, T. Cramer, and B. Fraboni, "Ionic Solvent Shell Drives Electroactuation in Organic Mixed Ionic-Electronic Conductors," *Advanced Science* 11 (2024): e2308746.

26424169, 2025, 21, Downloaded from https://onlinelibrary.wiley.com/doi/10.1002/pol.20250064 by Universitaet Bayreuth, Wiley Online Library on [10/03/2026]. See the Terms and Conditions (https://onlinelibrary.wiley.com/terms-and-conditions) on Wiley Online Library for rules of use; OA articles are governed by the applicable Creative Commons License

15. S. S. Nakshatharan, J. G. Martinez, A. Punning, A. Aabloo, and E. W. H. Jager, "Soft Parallel Manipulator Fabricated by Additive Manufacturing," *Sensors and Actuators B: Chemical* 305 (2020): 127355.

16. G. Dijk, H. J. Ruigrok, and R. P. O'connor, "Influence of PEDOT:PSS Coating Thickness on the Performance of Stimulation Electrodes," *Advanced Materials Interfaces* 7, no. 16 (2020): 42, https://doi.org/10.1002/admi.202000675.

17. D. A. Koutsouras, P. Gkoupidenis, C. Stolz, V. Subramanian, G. G. Malliaras, and D. C. Martin, "Impedance Spectroscopy of Spin-Cast and Electrochemically Deposited PEDOT:PSS Films on Microfabricated Electrodes With Various Areas," *ChemElectroChem* 4 (2017): 2321–2327.

18. J. Li, J. Cao, B. Lu, and G. Gu, "3D-Printed PEDOT:PSS for Soft Robotics," *Nature Reviews Materials* 8 (2023): 604–622.

19. C. Zhang, L. Margotti, F. Decataldo, et al., "Organic Mixed Ionic Electronic Conductor Nanochannels for Vertical Electrochemical and Ionic Transistors," *Advanced Electronic Materials* 10 (2024): 2300762.

20. I. Põldsalu, K. Rohtlaid, T. M. G. Nguyen, et al., "Thin Ink-Jet Printed Trilayer Actuators Composed of PEDOT:PSS on Interpenetrating Polymer Networks," *Sensors and Actuators B: Chemical* 258 (2018): 1072–1079.

21. J. Gladisch, V. K. Oikonomou, M. Moser, et al., "An Electroactive Filter With Tunable Porosity Based on Glycolated Polythiophene," *Small Science* 2, no. 4 (2022): 2100113, https://doi.org/10.1002/smsc.202100113.

22. C. Prönnecke, M. Staude, R. Frank, H. G. Jahnke, and A. A. Robitzki, "Electrically Switchable Monostable Actuatoric Polymer-Based Nanovalve Arrays With a Long-Term Stability," *Nano Letters* 18 (2018): 6375–6380.

23. A. Gelmi, M. J. Higgins, and G. G. Wallace, "Physical Surface and Electromechanical Properties of Doped Polypyrrole Biomaterials," *Biomaterials* 31 (2010): 1974–1983.

24. M. J. Higgins, S. T. Mcgovern, and G. G. Wallace, "Visualizing Dynamic Actuation of Ultrathin Polypyrrole Films," *Langmuir* 25 (2009): 3627–3633.

25. C. Puckert, E. Tomaskovic-Crook, S. Gambhir, G. G. Wallace, J. M. Crook, and M. J. Higgins, "Electro-Mechano Responsive Properties of Gelatin Methacrylate (GelMA) Hydrogel on Conducting Polymer Electrodes Quantified Using Atomic Force Microscopy," *Soft Matter* 13 (2017): 4761–4772.

26. M. S. Ting, B. N. Narasimhan, J. Travas-Sejdic, and J. Malmström, "Soft Conducting Polymer Polypyrrole Actuation Based on Poly(N-Isopropylacrylamide) Hydrogels," *Sensors and Actuators B: Chemical* 343 (2021): 130167.

27. E. Smela and N. Gadegaard, "Volume Change in Polypyrrole Studied by Atomic Force Microscopy," *Journal of Physical Chemistry B* 105 (2001): 9395–9405.

28. S. E. Feicht, G. D. Degen, and A. S. Khair, "Moving Ion Fronts in Mixed Ionic-Electronic Conducting Polymer Films," *AICHE Journal* 61 (2015): 1447–1454.

29. J. Rivnay, S. Inal, B. A. Collins, et al., "Structural Control of Mixed Ionic and Electronic Transport in Conducting Polymers," *Nature Communications* 7 (2016): 11287.

30. E. Stavrinidou, P. Leleux, H. Rajaona, et al., "Direct Measurement of Ion Mobility in a Conducting Polymer," *Advanced Materials* 25 (2013): 4488–4493.

31. E. Stavrinidou, M. Sessolo, B. Winther-Jensen, S. Sanaur, and G. G. Malliaras, "A Physical Interpretation of Impedance at Conducting Polymer/Electrolyte Junctions," *AIP Advances* 4, no. 4 (2014): 017127.

32. C. Dingler, R. Walter, B. Gompf, and S. Ludwigs, "In Situ Monitoring of Optical Constants, Conductivity, and Swelling of PEDOT:PSS From Doped to the Fully Neutral State," *Macromolecules* 55 (2022): 1600–1608.

33. L. G. Kaake, B. Gompf, and S. Ludwigs, "Electrochemical and Solvent-Driven Swelling in a Conducting Polymer Film," *Chemistry of Materials* 35 (2023): 4532–4540.

34. M. Eickenscheidt, E. Singler, and T. Stieglitz, "Pulsed Electropolymerization of PEDOT Enabling Controlled Branching," *Polymer Journal* 51 (2019): 1029–1036.

35. W. J. Feast, J. Tsibouklis, K. L. Pouwer, L. Groenendaal, and E. W. Meijer, "Synthesis, Processing and Material Properties of Conjugated Polymers," *Polymer* 37 (1996): 5017–5047.

36. V. Kuznetsov and G. Papastavrou, "Ion Adsorption on Modified Electrodes as Determined by Direct Force Measurements Under Potentiostatic Control," *Journal of Physical Chemistry C* 118 (2014): 2673–2685.

37. P. Knittel, H. Zhang, C. Kranz, G. G. Wallace, and M. J. Higgins, "Probing the PEDOT:PSS/Cell Interface With Conductive Colloidal Probe AFM-SECM," *Nanoscale* 8 (2016): 4475–4481.

38. H. Mousavi, L. M. Ferrari, A. Whiteley, and E. Ismailova, "Kinetics and Physicochemical Characteristics of Electrodeposited PEDOT:PSS Thin Film Growth," *Advanced Electronic Materials* 9 (2023): 7.

39. N. Raßmann, M. Weber, R. E. J. Glaß, et al., "Electrogelation: Controlled Fast Formation of Micrometer-Thick Films From Low-Molecular Weight Hydrogelators," *Langmuir* 39 (2023): 17190–17200.

40. V. Castagnola, C. Bayon, E. Descamps, and C. Bergaud, "Morphology and Conductivity of PEDOT Layers Produced by Different Electrochemical Routes," *Synthetic Metals* 189 (2014): 7–16.

41. U. Lang, E. Müller, N. Naujoks, and J. Dual, "Microscopical Investigations of PEDOT:PSS Thin Films," *Advanced Functional Materials* 19 (2009): 1215–1220.

42. F. Hu, Y. Xue, J. Xu, and B. Lu, "PEDOT-Based Conducting Polymer Actuators," *Frontiers in Robotics and AI* 6 (2019): 114.

43. J. G. Martinez, T. F. Otero, and E. W. Jager, "Effect of the Electrolyte Concentration and Substrate on Conducting Polymer Actuators," *Langmuir* 30 (2014): 3894–3904.

44. T. F. Otero and J. Padilla, "Anodic Shrinking and Compaction of Polypyrrole Blend: Electrochemical Reduction Under Conformational Relaxation Kinetic Control," *Journal of Electroanalytical Chemistry* 561 (2004): 167–171.

45. H. J. Butt, "Measuring Electrostatic, Van der Waals, and Hydration Forces in Electrolyte Solutions With an Atomic Force Microscope," *Biophysical Journal* 60 (1991): 1438–1444.

46. W. A. Ducker, T. J. Senden, and R. M. Pashley, "Direct Measurement of Colloidal Forces Using an Atomic Force Microscope," *Nature* 353 (1991): 239–241.

47. V. Kuznetsov and G. Papastavrou, "Note: Mechanically and Chemically Stable Colloidal Probes From Silica Particles for Atomic Force Microscopy," *Review of Scientific Instruments* 83 (2012): 116103.

48. G. Meyer and N. M. Amer, "Novel Optical Approach to Atomic Force Microscopy," *Applied Physics Letters* 53 (1988): 1045–1047.

49. K. Tybrandt, I. V. Zozoulenko, and M. Berggren, "Chemical Potential–Electric Double Layer Coupling in Conjugated Polymer–Polyelectrolyte Blends," *Science Advances* 3 (2017): eaao3659.

50. E. Stavrinidou, P. Leleux, H. Rajaona, M. Fiocchi, S. Sanaur, and G. G. Malliaras, "A Simple Model for Ion Injection and Transport in Conducting Polymers," *Journal of Applied Physics* 113 (2013): 24.

51. R. Wu, B. D. Paulsen, Q. Ma, and J. Rivnay, "Mass and Charge Transport Kinetics in an Organic Mixed Ionic–Electronic Conductor," *Chemistry of Materials* 34 (2022): 9699–9710.

52. T. Sedghamiz, A. Y. Mehandzhiyski, M. Modarresi, M. Linares, and I. Zozoulenko, "What Can We Learn About PEDOT:PSS Morphology From Molecular Dynamics Simulations of Ionic Diffusion?," *Chemistry of Materials* 35 (2023): 5512–5523.

26424169, 2025, 21, Downloaded from https://onlinelibrary.wiley.com/doi/10.1002/pol.20250064 by Universitaet Bayreuth, Wiley Online Library on [10/03/2026]. See the Terms and Conditions (https://onlinelibrary.wiley.com/terms-and-conditions) on Wiley Online Library for rules of use; OA articles are governed by the applicable Creative Commons License

53. S. E. Feicht, O. Schnitzer, and A. S. Khair, "Asymptotic Analysis of Double-Carrier, Space-Charge-Limited Transport in Organic Light-Emitting Diodes," *Proceedings of the Royal Society A: Mathematical, Physical and Engineering Sciences* 469 (2013): 20130263.

54. A. V. Volkov, K. Wijeratne, E. Mitraka, et al., "Understanding the Capacitance of PEDOT:PSS," *Advanced Functional Materials* 27, no. 28 (2017): 1700329, https://doi.org/10.1002/adfm.201700329.

55. V. Kaphle, P. R. Paudel, D. Dahal, R. K. Radha Krishnan, and B. Lüssem, "Finding the Equilibrium of Organic Electrochemical Transistors," *Nature Communications* 11 (2020): 2515.

56. H. Yang, E. Glynos, B. Huang, and P. F. Green, "Out-Of-Plane Carrier Transport in Conjugated Polymer Thin Films: Role of Morphology," *Journal of Physical Chemistry C* 117 (2013): 9590–9597.

57. J. Bobacka, A. Lewenstam, and A. Ivaska, "Electrochemical Impedance Spectroscopy of Oxidized Poly(3,4-Ethylenedioxythiophene) Film Electrodes in Aqueous Solutions," *Journal of Electroanalytical Chemistry* 489 (2000): 17–27.

58. A. C. Lazanas and M. I. Prodromidis, "Electrochemical Impedance Spectroscopy—A Tutorial," *ACS Measurement Science Au* 3 (2023): 162–193.

59. M. E. Orazem and B. Tribollet, *Electrochemical Impedance Spectroscopy* (John Wiley an Sons, 2017).

60. J. Bisquert, G. Garcia-Belmonte, P. Bueno, E. Longo, and L. O. S. Bulhões, "Impedance of Constant Phase Element (CPE)-Blocked Diffusion in Film Electrodes," *Journal of Electroanalytical Chemistry* 452, no. 2 (1998): 229–234, https://doi.org/10.1016/S0022-0728(98)00115-6.

61. A. Wang, D. Jung, D. Lee, and H. Wang, "Impedance Characterization and Modeling of Subcellular to Micro-Sized Electrodes With Varying Materials and PEDOT:PSS Coating for Bioelectrical Interfaces," *ACS Applied Electronic Materials* 3 (2021): 5226–5239.

62. F. Bonafè, C. Dong, G. G. Malliaras, T. Cramer, and B. Fraboni, "Subsurface Profiling of Ion Migration and Swelling in Conducting Polymer Actuators With Modulated Electrochemical Atomic Force Microscopy," *ACS Applied Materials and Interfaces* 16 (2024): 36727–36734.

63. C. Boehler, F. Oberueber, and M. Asplund, "Tuning Drug Delivery From Conducting Polymer Films for Accurately Controlled Release of Charged Molecules," *Journal of Controlled Release* 304 (2019): 173–180.

64. J. L. Hutter and J. Bechhoefer, "Calibration of Atomic-Force Microscope Tips," *Review of Scientific Instruments* 1993 (1868): 64–1873.

65. F. Berg, S. Block, S. Drache, R. Hippler, and C. A. Helm, "Effects of Reactive Oxygen Species on Single Polycation Layers," *Journal of Physical Chemistry. B* 117 (2013): 8475–8483.

Supporting Information

Additional supporting information can be found online in the Supporting Information section.

26424169, 2025, 21, Downloaded from https://onlinelibrary.wiley.com/doi/10.1002/pol.20250064 by Universitaet Bayreuth, Wiley Online Library on [10/03/2026]. See the Terms and Conditions (https://onlinelibrary.wiley.com/terms-and-conditions) on Wiley Online Library for rules of use; OA articles are governed by the applicable Creative Commons License